Resonant Modes of a Dielectric Rod Resonator Short-Circuited at Both Ends by Parallel Conducting Plates

YOSHIO KOBAYASHI, MEMBER, IEEE, AND SHUZO TANAKA, SENIOR MEMBER, IEEE

Abstract—**This paper describes a generalized study for the resonant modes of a dielectric rod resonator placed between two parallel conducting plates. Dielectric and conductor losses are ignored. It is shown that there are two resonant states in this resonator, trapped and leaky states. In order to determine the cutoff and resonant frequencies in the trapped state, numerical results are given for the cutoff conditions and dispersive characteristics of a dielectric rod waveguide. The field patterns for the hybrid modes are also presented. For the resonant modes in the leaky state, it is shown to be useful to introduce a complex angular frequency. Numerical results are given for the various modes with different values of the dielectric constant. Generalized mode charts covering both states and including the cutoff conditions are presented. The existence of both states has been verified by experiments.**

I. Introduction

THIS PAPER discusses the resonant modes of the dielectric rod resonator shown in Fig. 1. Here, a cylindrical dielectric rod having relative dielectric constant ϵ_r, diameter D, and length L is placed between two infinite parallel conducting plates. Dielectric and conductor losses are ignored. The configuration is important for applications such as the precise measurement of high-ϵ_r materials [1]–[5], and the design of waveguide Y-junction circulators containing full height ferrite rod [6].

It is well known that trapped and leaky waves propagate along a dielectric rod waveguide [7]–[9] and along other surface wave lines [10], [11]. By analogy with this, we assert in this paper that there are two resonant states in this resonator, trapped and leaky states. In the trapped state, the energy is confined in and near the rod; the unloaded quality factor Q_u is infinite. On the other hand, in the leaky state a part of the energy leaks away from the resonator in the radial direction; the Q_u value is finite due to the radiation loss even in the lossless structure.

In order to determine the cutoff and resonant frequencies in the trapped state, we first present numerical results for the cutoff conditions and dispersive characteristics of the dielectric rod waveguide. The field patterns for the hybrid modes are also calculated using these results. These calculations are based on the analysis by Snitzer [12]. Secondly, the solutions in the leaky state are calculated numerically by introducing a complex angular frequency. The same approach has been applied by Gastine *et al.* [13], to the analysis for a spherical dielectric resonator. Thirdly, generalized mode charts covering both states and including the cutoff conditions are presented. The mode charts presented previously [3], [5], [14], [15] include only the resonances in the trapped state. Finally, experimental results for the resonators are discussed to confirm the validity of the theory.

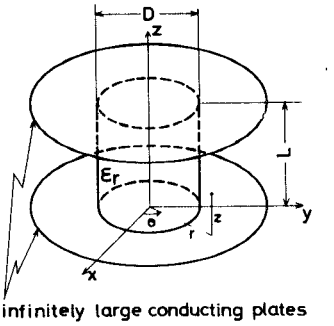

Fig. 1. A cylindrical dielectric rod resonator placed between two parallel conducting plates.

II. Characteristic Equations of Resonant Modes

If we choose a cylindrical coordinate system r, θ, z as in Fig. 1 and assume a time factor $\exp^{j\omega t}$, where ω is the angular frequency, then the characteristic equation for the resonant modes HE_{nml} and EH_{nml} is given by [16]

$$[F_n(u)+M_n(v)][k_1^2F_n(u)+k_2^2M_n(v)]=n^2h^2\left(\frac{1}{u^2}-\frac{1}{v^2}\right)^2 \tag{1}$$

where

$$F_n(u)=\frac{J_n'(u)}{uJ_n(u)} \qquad M_n(v)=-\frac{H_n^{(2)\prime}(v)}{vH_n^{(2)}(v)} \tag{2}$$

$$u=\frac{D}{2}\sqrt{k_1^2-h^2} \qquad v=\frac{D}{2}\sqrt{k_2^2-h^2} \tag{3}$$

$$k_1=\frac{\omega}{c}\sqrt{\epsilon_r} \qquad k_2=\frac{\omega}{c} \tag{4}$$

$$h=\frac{2\pi}{\lambda_g}=\frac{\pi l}{L}, \qquad l=0,1,2,\cdots. \tag{5}$$

Manuscript received April 3, 1980; revised June 12, 1980.

Y. Kobayashi is with the Department of Electrical Engineering, Saitama University, Urawa, Saitama 338, Japan.

S. Tanaka is with the Department of Electronics Engineering, Saitama Institute of Technology, Okabe, Saitama 369-09, Japan.

0018-9480/80/1000-1077$00.75

$J_n(u)$ is the Bessel function of the first kind and $H_n^{(2)}(v)$ is the Hankel function of the second kind. The prime above a cylinder function denotes differentiation with respect to the argument. Also, c is the light velocity in free space, and λ_g is the guiding wavelength of the dielectric rod waveguide. Equation (5) holds since the resonance occurs when $L=l\lambda_g/2$. In the case of either $n=0$ or $l=0$, particularly, (1) reduces to two equations: for the TE_{0ml} ($n=0$) and TE_{nm0} ($l=0$) modes

$$F_n(u)+M_n(v)=0 \tag{6}$$

and for the TM_{0ml} ($n=0$) and TM_{nm0} ($l=0$) modes

$$\epsilon_r F_n(u)+M_n(v)=0. \tag{7}$$

In addition, the TE_{nm0} mode disappears since it violates the short-circuit boundary conditions at both ends of the resonator. The designation of the resonant modes described above is based on that of the dielectric waveguide modes proposed by Snitzer [12]. The mode subscripts n, m, l are positive integers; the first two denote the waveguide mode, while the third one denotes the number of the field variations along z direction. The mode subscript 0 denotes no field variation.

In this resonator two states of the resonances should be considered. First, when u is real and v is imaginary in (3), that is, $\sqrt{\epsilon_r} > (\lambda_0 l/2L) \geq 1$ with the free-space wavelength λ_0 corresponding to the resonant frequency f_0, the resonances are in the trapped state. The state of $\lambda_0 l/2L = 1$, particularly, is called cutoff as is done for the dielectric waveguide. In this case the second equations in (2) and (3) reduce to

$$M_n(-jw)=\frac{K_n'(w)}{wK_n(w)} \tag{8}$$

$$v=-jw=-j\frac{D}{2}\sqrt{h^2-k_2^2} \tag{9}$$

where $K_n(w)$ is the modified Bessel function of the second kind with the real argument w. Secondly, when $1 > (\lambda_0 l/2L) \geq 0$, the resonances are in the leaky state. The TM_{nm0} modes are always in the leaky state since $l=0$. Equations (1), (6), and (7) can be solved by introducing a complex angular frequency ω

$$\omega=\omega_1+j\omega_2=\omega_1\left(1+j\frac{1}{2Q_f}\right), \qquad Q_f=\frac{\omega_1}{2\omega_2} \tag{10}$$

where ω_1 and ω_2 are both positive for the so-called damped free oscillation, and Q_f is its quality factor [17]. Then u and v are both complex. Putting $v=v_1+jv_2$, we obtain the following relation from the imaginary part of the second of (3):

$$\frac{\omega_1\omega_2}{c^2}-\frac{v_1v_2}{(D/2)^2}=0. \tag{11}$$

Since v_1 is positive for the wave travelling in the r direction, v_2 is positive by (11). Therefore it is sufficient here to examine only the first quadrant of the complex v plane. From the above discussion it follows that for a given real h value, ω which is determined from the characteristic equation is real in the trapped state and is complex in the leaky state. This is in contrast with the case of the dielectric waveguide where for a given real ω value, the propagation constant h determined is real in the trapped wave and is complex in the leaky wave [7]–[11].

III. Calculations of Trapped Wave of a Dielectric Rod Waveguide

As the basic investigation for understanding the resonant behavior in the trapped state, a systematic study was made of the trapped waves for the dielectric rod waveguide. The results will be described below.

A. Cutoff Condition

At the cutoff of the trapped wave, $w=0$ and $\lambda_c/\lambda_g=1$, where λ_c is the cutoff wavelength; hence the first of (3) becomes $u_c=(\pi D/\lambda_c)\sqrt{\epsilon_r-1}$. Define X and Y as

$$X=\frac{D}{\lambda_c}\sqrt{\epsilon_r}=\frac{u_c}{\pi}\frac{1}{\sqrt{1-Y^2}} \qquad Y=\frac{1}{\sqrt{\epsilon_r}} \tag{12}$$

where u_c values are given by the following cutoff conditions [12]:

$$\begin{aligned}
&HE_{11}: && u_c=0\\
&TE_{0m} \text{ and } TM_{0m}: && J_0(u_c)=0\\
&EH_{1m} \text{ and } HE_{1\,m+1}: && J_1(u_c)=0\\
&EH_{nm}\ (n=2,3,\cdots): && J_n(u_c)=0\\
&HE_{nm}\ (n=2,3,\cdots): && u_c\frac{J_{n-2}(u_c)}{J_{n-1}(u_c)}=-(n-1)(\epsilon_r-1).
\end{aligned} \tag{13}$$

The relationship between X and Y for each mode, calculated from (12) and (13), is shown in Fig. 2, which constitutes a complete set of the trapped waves. With reference to Fig. 2, this verification can be made as follows. The cutoff for the TE_{01} and TM_{01} modes starts from the point $X=0.765$ and $Y=0$; as $Y\to 1$, it approaches to the HE_{21} cutoff; furthermore, as $Y\to 0$, the latter reaches the EH_{11} and HE_{12} cutoff; continuously, as $Y\to 1$, the latter approaches to the HE_{31} cutoff; repeating the above procedure, we obtain a sequence of the modes for $m=1$. Similarly we get another sequence for $m=2$ starting from the point $X=1.76$ and $Y=0$, and a sequence for $m=m$, generally, starting from the point $X=$(the mth root of $J_0(u_c)=0)/\pi$ and $Y=0$. Table I summarizes these results. The cutoff for the HE_{11} mode is specially considered and added to the modes in Table I. The necessary X value is readily determined from Fig. 2 for each mode with given ϵ_r.

B. Solutions of Characteristic Equations

In order to calculate the hybrid modes, it is convenient to introduce a function P defined by Snitzer [12], which represents the amount of the field component H_z relative

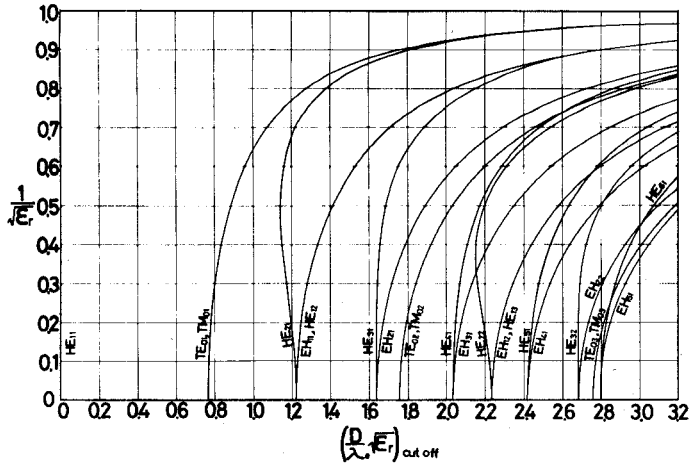

Fig. 2. Cutoff conditions for trapped waves of a dielectric rod waveguide.

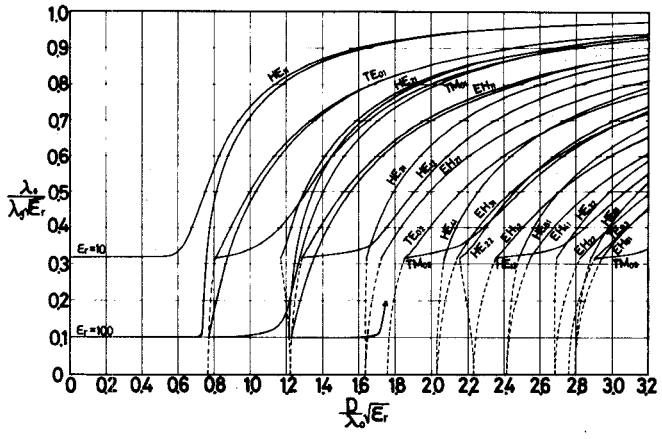

Fig. 3. Dispersion relation for the trapped waves of a dielectric rod waveguide in the cases of $\epsilon_r = 10$ and 100.

TABLE I
CLASSIFICATION OF TRAPPED WAVES BY MEANS OF CUTOFF CURVES

	X at Y=0	Y=0 →	Y=1 →	Y=0 →	Y=1 →	Y=0 →	Y=1 →	Y=0 →	Y=1 →
m=1	0.765	TE_{01}, TM_{01}	HE_{21}	EH_{11}, HE_{12}	HE_{31}	EH_{21}	HE_{41}	EH_{31}	HE_{51}
m=2	1.757	TE_{02}, TM_{02}	HE_{22}	EH_{12}, HE_{13}	HE_{32}	EH_{22}	HE_{42}	EH_{32}	HE_{52}
m=m	u_c/π^*	TE_{0m}, TM_{0m}	HE_{2m}	EH_{1m}, HE_{1m+1}	HE_{3m}	EH_{2m}	HE_{4m}	EH_{3m}	HE_{5m}

* u_c is the m'th root of $J_0(u_c)=0$.

to that of E_z. Then we rewrite (1) as follows:

$$P = \frac{n\left(\frac{1}{u^2}+\frac{1}{w^2}\right)}{F_n(u)+M_n(-jw)} = \frac{k_1^2 F_n(u)+k_2^2 M_n(-jw)}{nh^2\left(\frac{1}{u^2}+\frac{1}{w^2}\right)}. \quad (14)$$

The dispersion relations for the trapped waves were calculated numerically using (6), (7), and (14) together with (8) and (9). Results for several modes with $\epsilon_r = 10$ and 100 are shown in Fig. 3 by the solid lines. The broken lines in Fig. 3 indicate the cutoffs in the range $\epsilon_r \geq 10$, taken from Fig. 2. Furthermore, the P values for $\epsilon_r = 10$ are plotted in Fig. 4. With reference to Fig. 4, it is found

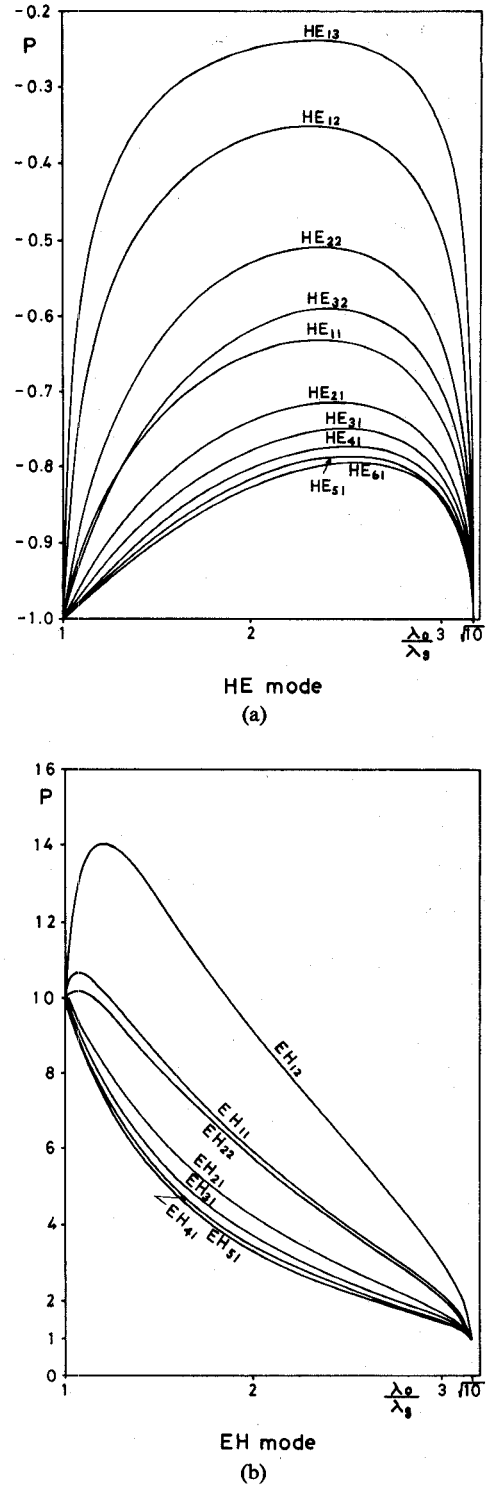

Fig. 4. The values of P versus λ_0/λ_g for the hybrid modes in the case of $\epsilon_r = 10$. (a) HE_{nm} mode. (b) EH_{nm} mode.

that for the HE mode the TM mode is predominant since $|P|<1$ and for the EH mode the TE mode is predominant since $|P|>1$ [15].

C. Field Patterns for Hybrid Modes

Fig. 5 shows the field patterns of the hybrid modes for the fixed values of $\epsilon_r = 10$ and $\lambda_0/\lambda_g = 2.6$. They were calculated from the equations given in reference [12, eq.

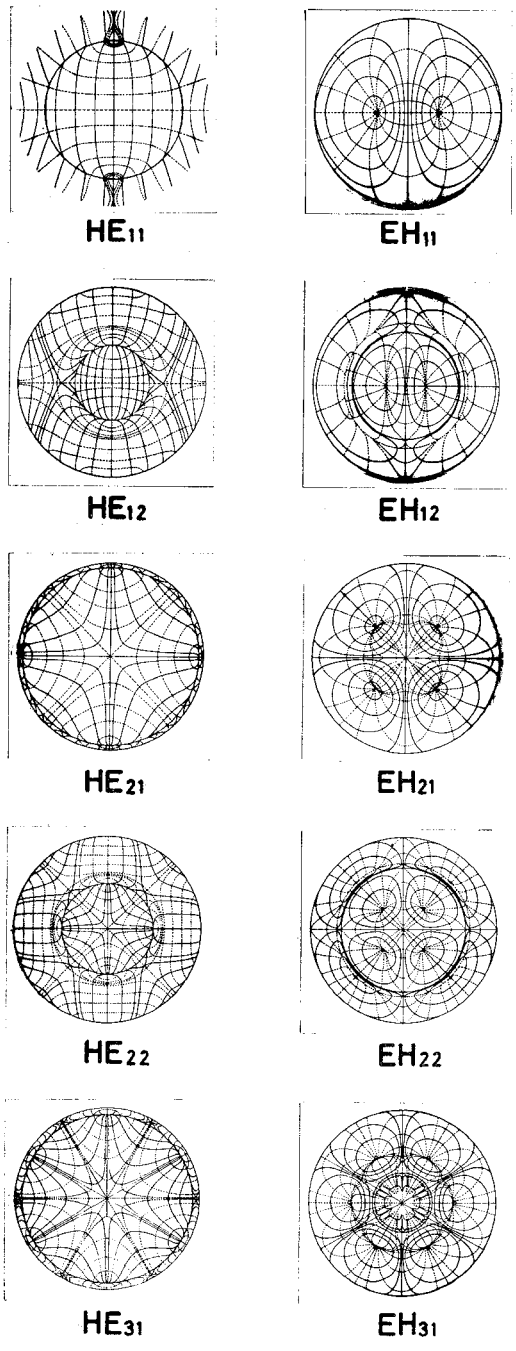

Fig. 5. Field patterns for the hybrid modes of a dielectric rod waveguide when $\epsilon_r = 10$ and $\lambda_0/\lambda_g = 2.6$. —— Electric field line. ····· Magnetic field line.

(17)], together with the values of P and D/λ_0 given in Figs. 3 and 4. The transverse view is in the plane where $E_z = H_z = 0$. The patterns only inside the rod are presented for all the modes except the HE_{11} mode. It should be noted that the curvature of the field lines for the HE_{11} mode is the opposite direction to that commonly assumed, e.g., [16]. This fact has been recognized by Nagelberg and Hoffspiegel [18].

The field patterns for the HE_{nm} and EH_{nm} modes have a strong resemblance to those for the TM_{nm} and TE_{nm} modes in an assumed magnetic-wall waveguide, respectively [19]. Furthermore, interchanging the electric and magnetic field lines in the latter waveguide modes, we get the familiar metallic-wall waveguide modes TE_{nm} and TM_{nm}, respectively. Thus, these three types of the waveguide modes can be explicitly correlated one another. From this point of view, the mode designation by Snitzer [12] is more reasonable than that by Kikuchi and Yamashita [20].

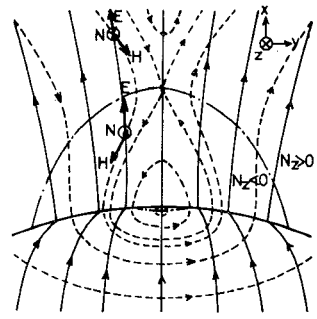

Fig. 6. Region of negative power flow for HE_{11} mode when $\epsilon_r = 10$ and $\lambda_0/\lambda_g = 2.6$.

Fig. 6 shows a detail of the upper part of the HE_{11} mode pattern. In the figure arrows on the field lines are so directed that the Poynting vector $\boldsymbol{N} = \boldsymbol{E} \times \boldsymbol{H}$ points in the positive z direction. In the region enclosed by the dot-dash-line, however, $\boldsymbol{N}$ points in the negative z direction. This phenomenon for the negative power flow has been found by Gillespie [21]. Furthermore it has been found that the phenomenon for the HE_{11} mode appears in the range $1.23 < \lambda_0/\lambda_g < 2.99$ when $\epsilon_r = 10$ [22] and disappears everywhere if $\epsilon_r < 7.34$ [23].

The field patterns in Fig. 5 are applicable to those for the resonant modes without modification, if we note that the electric and magnetic field lines are 90° out of phase with each other both in time and in space along z axis.

IV. TM_{nm0} Leaky State Modes

Using the formula $xZ_n'(x) = -nZ_n(x) + xZ_{n-1}(x)$ where $Z_n(x)$ is $J_n(x)$ or $H_n^{(2)}(x)$, we can rewrite (7) for the TM_{nm0} mode as follows:

$$u\frac{J_{n-1}(u)}{J_n(u)} = v\frac{H_{n-1}^{(2)}(v)}{H_n^{(2)}(v)} \tag{15}$$

where it follows from (3)–(5), and (10) that

$$u = \sqrt{\epsilon_r}\, v \qquad v = \frac{D\omega}{2c} = \frac{\pi D}{\lambda_0}\left(1 + j\frac{1}{2Q_f}\right) = V\angle\theta \tag{16}$$

and V and θ are the amplitude and phase of the complex number v, respectively. For fixed values of n and ϵ_r, (15) was solved for v by a computer with the subprogram of the complex Bessel functions [24]. Let $V_{nm}\angle\theta_{nm}$ be the solution for the TM_{nm0} modes; then the resultant values of u_{nm} and Q_{fnm} given by

$$u_{nm} = \frac{\pi D}{\lambda_0}\sqrt{\epsilon_r} = \sqrt{\epsilon_r}\, V_{nm}\cos\theta_{nm} \qquad Q_{fnm} = \frac{1}{2}\cot\theta_{nm} \tag{17}$$

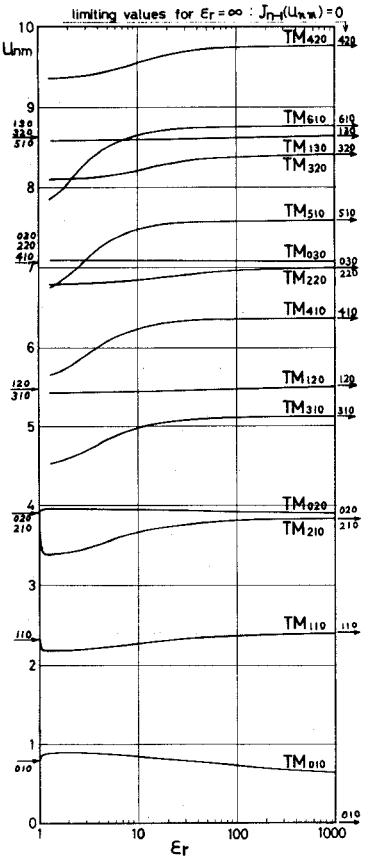

Fig. 7. The values of u_{nm} for TM_{nm0} leaky state modes.

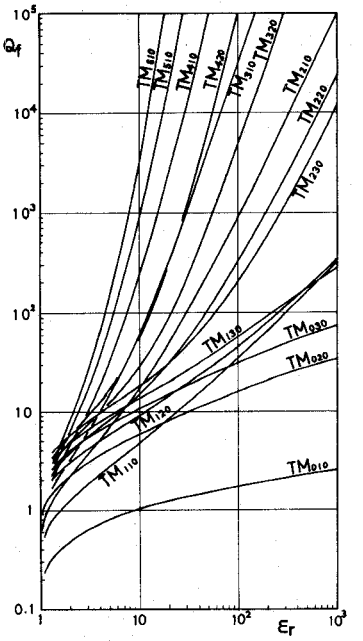

Fig. 8. The values of Q_{fnm} for TM_{nm0} leaky state modes.

are shown in Figs. 7 and 8. The solutions in the range $\epsilon_r < 1.3$ are presented for the four lowest-order modes only.

As $\epsilon_r \to 1$, asymptotic solutions u_{nm}^1 are given by (see Appendix)

$$u_{nm}^1 = \left(\frac{2n+1}{4} + m - 1\right)\pi \tag{18}$$

and are indicated in Fig. 7 on the left ordinate. It is found from (18) that the TM_{nm0} modes specified by the following suffices (n, m) are degenerate at $\epsilon_r = 1$; i.e., $(n,1)$, $(n-2,2)$, $(n-4,3), \cdots$, and $(n-2m-2,m)$ with $n-2m-2 \geqslant 0$. In the case of $n=5$, for example, the TM_{510}, TM_{320}, and TM_{130} modes are degenerate at $\epsilon_r = 1$ and have same values of $u = 8.639$. Also, asymptotic solutions u_{nm}^{∞} as $\epsilon_r \to \infty$ are given by (see Appendix)

$$J_{n-1}(u_{nm}^{\infty}) = 0 \tag{19}$$

which are indicated in Fig. 7 on the right ordinate. The $TM_{0,m+1,0}$ and TM_{2m0} modes are degenerate in the limit of $\epsilon_r \to \infty$. On the other hand, the different form has been commonly used so far, which is derived under the magnetic-wall assumption [25] and is given by

$$J_n'(u) = 0. \tag{20}$$

In the case of $n=0$, (19) and (20) happen to coincide. For all modes with $n \geqslant 1$, however, (19) provides much better approximation compared with (20) when ϵ_r is high; e.g., for the TM_{110} mode with $\epsilon_r = 100$, the errors of (19) and (20) are 1.5 and 22 percent, respectively. Furthermore, it has been found [6] that the treatment is applicable to the design of the waveguide Y-junction circulator. With the reference to Fig. 8, the Q_f values increase with the increase of ϵ_r or n, but decrease with the increase of m.

V. Mode Chart Covering Both States

Fig. 9 shows a mode chart for the resonator illustrated in Fig. 1, including the trapped state modes, their cutoff conditions, and the TM_{nm0} leaky state modes. The behavior below the cutoff of the resonant modes, i.e., that in the leaky state, will be discussed in Section VI. We choose $\epsilon_r(D/\lambda_0)^2$ as ordinate and $(D/L)^2$ as abscissa. This choice of the coordinate axes permits us to use the chart for the resonators with the different ϵ_r values [4], [5], [15], [24]. Examining the characteristic equation (1), we find that a solution, $\epsilon_r(D/\lambda_0)^2$, obtained for given values of n, m, ϵ_r, depends on the value of $(l/2)^2(D/L)^2$. Therefore the solutions for $l \geqslant 2$ can be readily found out from that for $l=1$. This relation holds for a pair of the leaky state solutions, $\epsilon_r(D/\lambda_0)^2$ and Q_f, too.

For the trapped state modes, the curves were plotted using Fig. 3 and the following relation:

$$\left(\frac{D}{L}\right)^2 = \left(\frac{2}{l}\right)^2 \left(\frac{\lambda_0}{\lambda_g \sqrt{\epsilon_r}}\right)^2 \left(\frac{D}{\lambda_0}\sqrt{\epsilon_r}\right)^2. \tag{21}$$

The solid lines are for $\epsilon_r = 10$ and the broken lines are for $\epsilon_r = 100$. The other modes existing in the upper-left region of the HE_{113} mode are omitted in the chart.

The cutoffs of the trapped state modes, depending on the ϵ_r value, can be expressed from (12) and (21) as

$$\epsilon_r \left(\frac{D}{\lambda_c}\right)^2 = \left(\frac{u_c}{\pi}\right)^2 \frac{\epsilon_r}{\epsilon_r - 1} \qquad \left(\frac{D}{L}\right)_c^2 = \left(\frac{2}{l}\right)^2 \left(\frac{u_c}{\pi}\right)^2 \frac{1}{\epsilon_r - 1}. \tag{22}$$

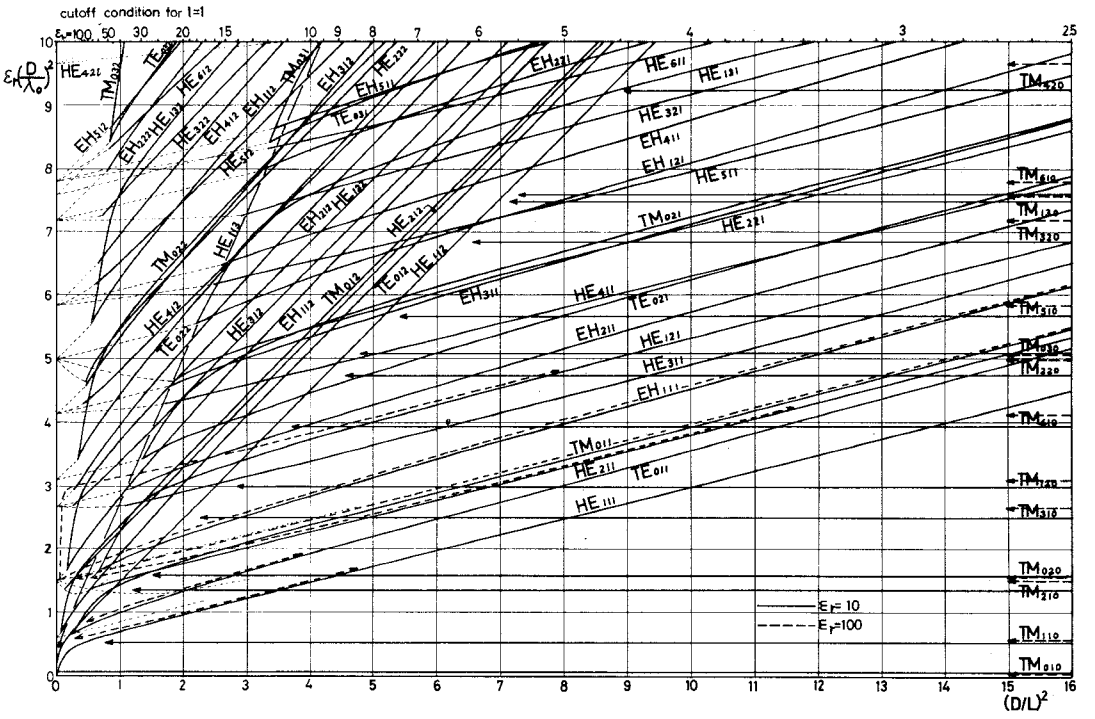

Fig. 9. Mode chart for a dielectric rod resonator short-circuited at the both ends.

Furthermore, the first of (22) subtracted by the second yields

$$\epsilon_r\left(\frac{D}{\lambda_c}\right)^2=\left(\frac{l}{2}\right)^2\left(\frac{D}{L}\right)_c^2+\left(\frac{u_c}{\pi}\right)^2 \tag{23}$$

which represents the straight line if u_c is independent of ϵ_r. Equation (22) for the HE_{nml} ($n\geqslant 2$) modes and (23) for the other modes, in the cases of $l=1$ and 2, are illustrated in Fig. 9 by the dotted lines. On the other hand, the first of (22) divided by the second yields another relation as follows:

$$\epsilon_r\left(\frac{D}{\lambda_c}\right)^2=\epsilon_r\left(\frac{l}{2}\right)^2\left(\frac{D}{L}\right)_c^2. \tag{24}$$

This represents a straight line which intersects the origin and has the slope of $(l/2)^2\epsilon_r$. Only the ϵ_r values satisfying (24) for $l=1$ are indicated on the top of the chart, while the straight lines are not drawn. In the chart we can determine the cutoffs for $l=1$ and given ϵ_r as follows; draw a straight line that connects the origin and the point ϵ_r on the top of the chart; the intersections of this line and the dotted lines for $l=1$ give the cutoffs for the corresponding modes. In addition, the cutoff points for all the modes with the different integers of only l lie on a straight line parallel to the abscissa.

The TM_{nm0} leaky state modes are indicated in the chart by the straight lines parallel to the abscissa, plotted using the relation $\epsilon_r(D/\lambda_0)^2=(u_{nm}/\pi)^2$ with the u_{nm} values given in Fig. 7. The parts beyond the arrows are omitted to avoid the confusion. If necessary, we can readily extend these lines.

In the following we describe how to use the chart. When $100\geqslant\epsilon_r\geqslant 10$, we can use it by interpolating between two curves for $\epsilon_r=10$ and 100. When $\epsilon_r>100$, the use of the curves for $\epsilon_r=100$ still provides a good approximation. Particularly in the vicinity of the cutoffs, the cutoff conditions described above should be taken into account. These considerations also permit us to use it even the the case of $\epsilon_r<10$. When the TE_{011} resonator is fabricated, for example, of the material of $\epsilon_r=2$, the TE_{011} cutoff condition requires us to use a rod having a size ratio of $(D/L)>1.55$. Furthermore, for the permittivity measurement using the TE_{0ml} mode [1]–[5], special attention should be paid to determine the sample size; e.g., for $\epsilon_r>10$, the use of $(D/L)^2\doteqdot 3$ should be avoided, because the leaky state modes TM_{020} and TM_{210} having the low Q_f values exist near the TE_{011} mode and disturb its fields.

VI. Transitions from Trapped-to-Leaky State

Fig. 10 shows the most generalized mode chart for $\epsilon_r=10$, covering both states and including the cutoff conditions. The trapped and leaky state modes are indicated by the light and heavy lines, respectively, The dotted lines are for the cutoffs. For the leaky state modes with $l\neq 0$, the numerical solutions were obtained from (1) to (7) together with (10), by an approach similar to that for the TM_{nm0} modes. For the other modes the curves were plotted from Fig. 9.

With decreasing $(D/L)^2$, for all the modes except the TM_{nm0} and HE_{1ml} modes the transitions from the trapped state to the leaky state occur at the cutoff points, as shown in Fig. 10(a), and their Q_f values decrease monotonically

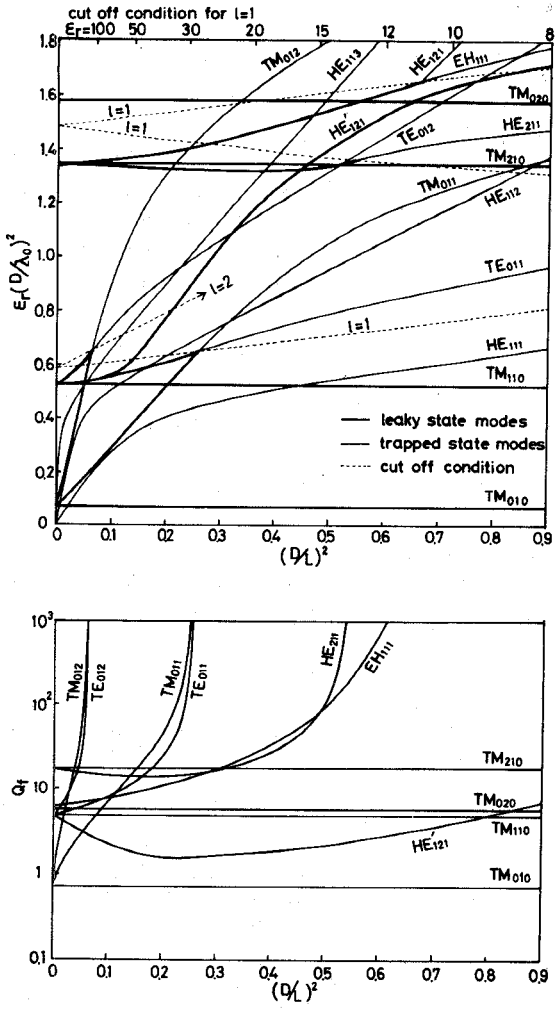

Fig. 10. The most generalized mode chart for $\epsilon_r=10$, covering both states and including cutoff conditions.

in the leaky state, as shown in Fig. 10(b). At $(D/L)^2=0$ the TM_{0ml} and HE_{nml} $(n\geq 2)$ modes coincide with the TM_{nm0} modes, while the TE_{0ml} and EH_{nml} modes coincide with the TE_{nm0} modes, because it is obvious from (5) that the infinite length L corresponds to $l=0$. Also, the TE_{0ml} modes coincide with the TM_{1m0} modes at $(D/L)^2=0$ since the TM_{1m0} and TE_{0m0} modes are always degenerate.

On the other hand, no transition of the HE_{121} trapped state mode into the leaky state was found from the calculation, while a distinct resonance which has the extremely low Q_f value and coincides with the TM_{110} mode at $(D/L)^2=0$ was found, as shown in Fig. 10. We call it HE'_{121} mode. Results calculated for $\epsilon_r=16$, 36, and 100 also showed the similar behavior for the HE_{121} and HE'_{121} modes. From these results it is expected that the HE_{1ml} modes are always in the trapped state.

VIII. Experimental Verification

The experiments for the resonant modes were carried out to verify the theory described above. The first resonator used was fabricated of a $(Zr-Sn)TiO_4$ ceramic rod of

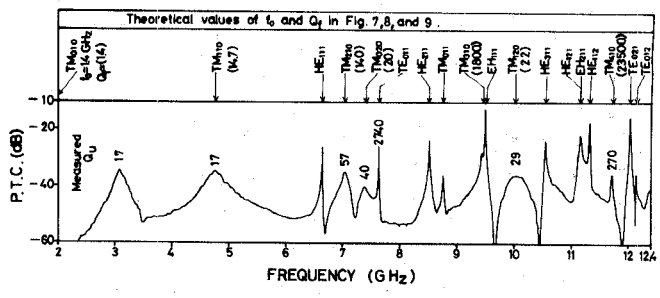

Fig. 11. Experiment for the identification of the resonant modes when $\epsilon_r=37.08$, $D=8.504$ mm, and $L=4.680$ mm, where PTC=power transmission coefficient.

$D=8.504$ mm and $L=4.680$ mm placed between two copper plates of 40 mm in diameter. This material has $\epsilon_r=37.08$ and $\tan\delta=1.6\times10^{-4}$ at 7.6 GHz. These values were measured using the TE_{011} mode. In order to reduce the air-gap effect on the resonant frequencies, small air gaps at the rod–plate interfaces were filled up with the least amount of water, whose dielectric constant is known nearly equal to that of the rod at microwave frequency. The frequency response of the transmission-type resonator was measured using a network analyzer. The result is shown in Fig. 11. Two coupling loops, each of which consists of a semirigid coaxial cable of the diameter 2.2 mm having a small loop at the top, were used to excite and detect both H_z and H_θ components of the resonant fields. The theoretical values of f_0 and Q_f estimated from Figs. 7, 8, and 9 are also indicated in Fig. 11. They are in good agreement with all the measured resonant peaks but the first one at 3.07 GHz. The first peak may be designated as the TM_{010} mode with the theoretical value of $f_0=1.4$ GHz, because it is known [17] that the difference between the resonant frequency for a forced oscillation and that for a damped free-oscillation increases with lower Q_f value. Furthermore the measured unloaded Q_u values for the TM_{nm0} leaky state modes are in fairly good agreement with the theoretical Q_f values in spite of the finite size of the conductor plates used here.

Second, in order to investigate the behavior in the vicinity of the cutoff for the TE_{011} mode, two resonators having the same diameters of $D=4.99$ mm and the different length were fabricated of the same materials as used above. In this experiment two coupling loops were oriented at right angle to each other to suppress the coupling strengths to the HE_{11l} modes appearing near the TE_{011} mode. The experimental results for both resonators are shown in Fig. 12(a) and (b). The resonant peaks were identified using the mode chart for $\epsilon_r=36$, shown in Fig. 12(c). For $L=18.91$ mm or $(D/L)^2=0.0696$, the TE_{011} mode is in the trapped state and has the measured Q_u value of 3500, as shown in Fig. 12(a), while for $L=20.92$ mm, or $(D/L)^2=0.569$, the TE_{011} mode is in the leaky state and its Q_u value decreases to 220 due to the radiation loss, as shown clearly in Fig. 12(b). Though the similar behavior for the TM_{011} mode was expected, the

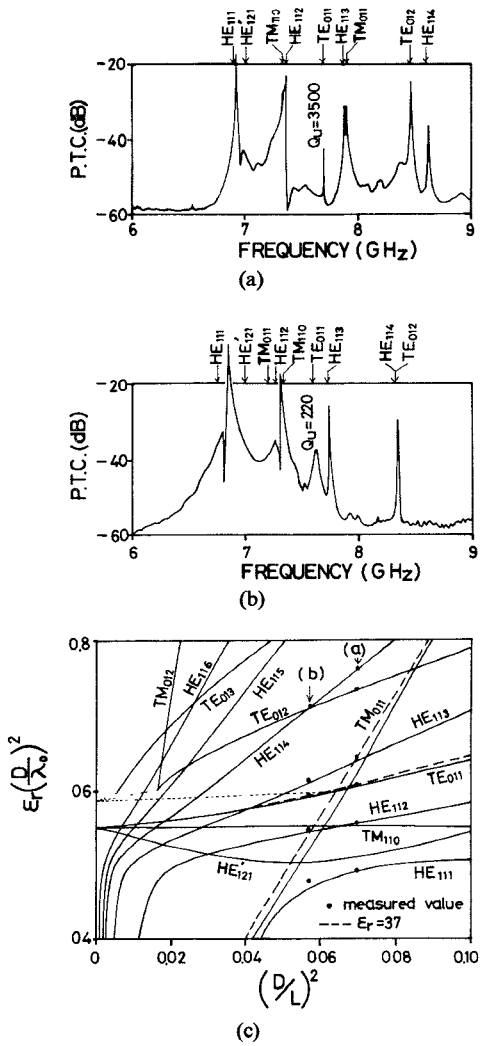

Fig. 12. Experiment of the identification of the resonant modes when $\epsilon_r=37.08$ and $D=4.99$ mm, where PTC=power transmission coefficient. (a) $L=18.91$ mm. (b) $L=20.92$ mm. (c) Mode chart for $\epsilon_r=36$.

evidence was not observed because of the poor mode separations, as shown in Fig. 12.

Appendix

Asymptotic Solutions for TM_{nm0} Modes

In the case of $\epsilon_r \to 1$, (16) is changed as follows:

$$u=v=\frac{D\omega}{2c}u^1\left(1+j\frac{1}{2Q_f}\right), \quad \text{with } u^1=\frac{D\omega_1}{2c}. \tag{A1}$$

With reference to (A1), u is needed to be infinite because of the physical consideration that $Q_f=0$ as $\epsilon_r \to 1$. Using the approximations of $J_n(u)$ and $H_n^{(2)}(u)$ for large value of argument u, we can obtain from (15) an asymptotic form

$$\tan\left(u-\frac{2n+1}{4}\pi\right)=j. \tag{A2}$$

Furthermore, substitution (A1) into (A2) leads to

$$\tan\left(u^1-\frac{2n+1}{4}\pi\right)=0$$

which yields (18).

In the following, we treat the case of $\epsilon_r \to \infty$. In order that u has a finite value as $\epsilon_r \to \infty$, v must vanish since $u=\sqrt{\epsilon_r}\,v$. Therefore an asymptotic value u^∞ can be obtained by solving (15) in the limit of $v \to 0$. When $v \to 0$, the right-hand side of (15) is zero for every integer of n. This calculation is straightforward, using the approximation of $H_n^{(2)}(v)$ for small argument v. As a result, we obtain (19). For $n=0$, the solution, $u_{01}^\infty=0$ can exist specially since $\lim_{u\to 0} uJ_1(u)/J_0(u)=0$. We call it TM_{010} mode.

Acknowledgment

The authors would like to thank Prof. N. Ogasawara of Tokyo Metropolitan University for helpful advices, and Prof. S. Yoshida of Saitama University for the encouragement. The authors also are indebted to M. Kato for his drafting assistance, and to M. Isono, T. Murui, N. Niijima, F. Suzuki, and S. Endo for their contributions with the calculations and experiments. The ceramic materials were presented by Murata Mfg. Co., Ltd.

References

[1] B. W. Hakki and P. D. Coleman, "A dielectric resonator method of measuring inductive capacities in the millimeter range," *IRE Trans. Microwave Theory Tech.*, vol. MTT-8, pp. 402–410, July 1960.

[2] S. B. Cohn and K. C. Kelly, "Microwave measurement of high dielectric constant materials," *IEEE Trans. Microwave Theory Tech.*, vol. MTT-14, pp. 406–410, Sept. 1966.

[3] W. E. Courtney, "Analysis and evaluation of a method of measuring the complex permittivity and permeability of microwave insulators," *IEEE Trans. Microwave Theory Tech.*, vol. MTT-18, pp. 476–485, Aug. 1970.

[4] Y. Kobayashi and S. Tanaka, "Discussions on dielectric resonator method of measuring complex dielectric constants," (in Japanese) *Trans. Inst. Electron Commun. Eng. Japan*, vol. 59-B, pp. 223–230, Apr. 1976.

[5] M. W. Pospieszalski, "On the theory and application of the dielectric post resonator," *IEEE Trans. Microwave Theory Tech.*, vol. MTT-25, pp. 228–231, Mar. 1977.

[6] Y. Akaiwa, "Operation modes of a waveguide *Y* circulator," *IEEE Trans. Microwave Theory Tech.*, vol. MTT-22, pp. 954–960, Nov. 1974.

[7] J. Arnbak, "Leaky waves on a dielectric rod," *Electron. Lett.*, vol. 5, pp. 41–42, 1969.

[8] J. R. James, "Leaky waves on a dielectric rod," *Electron. Lett.*, vol. 5, pp. 252–254, 1969.

[9] J. R. Wait, "Electromagnetic whispering gallery modes in a dielectric rod," *Radio Sci.*, vol. 2, pp. 1005–1017, 1967.

[10] F. J. Zucker, "The guiding and radiation of surface waves," in *Proc. Symp. Modern Advances in Microwave Techniques*, vol. 4 New York: Polytechnic Press, 1954, pp. 403–435.

[11] T. Tamir and A. A. Oliner, "Guided complex waves-pts. 1 and 2," *Proc. Inst. Elect. Eng.*, vol. 110, pp. 310–334, Feb. 1963.

[12] E. Snitzer, "Cylindrical dielectric waveguide modes," *J. Opt. Soc. Am.*, vol. 51, pp. 491–498, May 1961.

[13] M. Gastine, L. Courtois, and J. C. Dormann, "Electromagnetic resonances of free dielectric spheres," *IEEE Trans. Microwave Theory Tech.*, vol. MTT-15, pp. 694–700, Dec. 1967.

[14] D. L. Rebsch, D. C. Webb, R. A. Moore, and J. D. Cowlishow, "A mode chart for accurate design of cylindrical dielectric resonators," *IEEE Trans. Microwave Theory Tech.*, vol. MTT-13, pp. 468–469, Apr. 1965.

[15] Y. Kobayashi, "A mode chart for a cylindrical dielectric resonators," (in Japanese) Paper of Technical Group on Microwaves, IECE Japan, No. MW68-27, Aug. 1968.

[16] D. G. Kiely, *Dielectric Aerials*. New York: Wiley, 1953.

[17] J. C. Slater, *Microwave Electronics*. Princeton, NJ: Van Nostrand, 1950. p. 42.

[18] E. R. Nagelberg and J. N. Hoffspiegel, "Computer-graphic analy-

sis of dielectric waveguides," *IEEE Trans. Microwave Theory Tech.*, vol. MTT-15, pp. 187–189, Mar. 1967.
[19] N. Ogasawara and Y. Kobayashi, "Simplified calculation method for dielectric waveguide and resonator," (in Japanese) Paper of Technical Group on Microwaves, IECE Japan, No. TR63-18, Dec. 1963.
[20] H. Kikuchi and E. Yamashita, "Theory of dielectric waveguides and some experiments at 50 KMc," in *Proc. Symp. Millimeter Waves*. New York: Polytechnic Press, 1959, pp. 619–638.
[21] E. F. F. Gillespie, "Power flow and negative impedance in the dielectric rod waveguide," *Proc. Inst. Elect. Eng.*, vol. 107c, pp. 198–201, Feb. 1960.
[22] Y. Kobayashi, H. Shimamura, and Y. Kikukawa, "Negative Poynting vector for HE_{11} mode," (in Japanese) Nat. Conv. Rec. IECE Jap., No. 468, Sept. 1969.
[23] E. Yahagi, "Field distribution for HE_{11} mode," (in Japanese) Joint Conv. Rec. Four Inst. Electrical Engrs. Jap., No. 1285, Apr. 1970.
[24] Y. Kobayashi and S. Tanaka, "A mode chart for design of cylindrical dielectric rod resonators," *The Science and Engineering Reports of Saitama University*, vol. 9-c, pp. 24–30, 1975.
[25] H. M. Schlicke, "Quasi-degenerated modes in high-ϵ dielectric cavities," *J. Appl. Phys.*, vol. 24, pp. 187–191, Feb. 1953.

Dielectric Loaded Elliptical Waveguides

SEMBIAM R. RENGARAJAN, MEMBER, IEEE, AND J. E. LEWIS, SENIOR MEMBER, IEEE

***Abstract*—Wave propagation in a metallic elliptic waveguide loaded with a dielectric rod or a dielectric lining is investigated theoretically. The mode spectrum for both slow and fast wave hybrid modes is obtained by numerical solution of the characteristic equations. Correspondence is established between the modes of the loaded and unloaded elliptical waveguides. Typical field plots for $_eHE_{01}$ and $_eEH_{01}$ modes are presented. Power flow, power loss, and attenuation are obtained using a perturbation method.**

I. Introduction

THE DIELECTRIC loaded metallic elliptical waveguide has been shown to have application in acceleration devices [1], and also as a microwave heating applicator [2]. The study of metallic elliptical waveguides with two dielectric media involves the solution of an infinite determinantal equation. Veselov [3] derived the dispersion equations of all modes in this waveguide. Cutoff frequencies of some low-order modes, computed from a first-order approximation to the characteristic equation have been reported [4]–[7], while Rayevskiy *et al.* [8] have obtained the field distribution of the dominant mode. The dispersion equation of the $_eHE_{11}$ mode has been studied [9]–[11] for the special case of the phase velocity near the velocity of light because of its application in electron accelerators. The use of a second-order approximation to the dispersion equation has been reported to yield improved accuracy in the computation of cutoff frequencies and to reduce field mismatch errors [10]. The mode spectrum and propagation characteristics of this waveguide have not been reported previously.

Manuscript received March 4, 1980; revised June 24, 1980. This work was supported by the Natural Sciences and Engineering Research Council of Canada.

J. E. Lewis is with the Department of Electrical Engineering, University of New Brunswick, Fredericton, N.B. E3B 5A3, Canada.

S. R. Rengarajan was with the Department of Electrical Engineering, University of New Brunswick, Fredericton, N. B., E3B 5A3, Canada. He is now with the Electrical and Computer Engineering Department, California State University, Northridge, CA 91330.

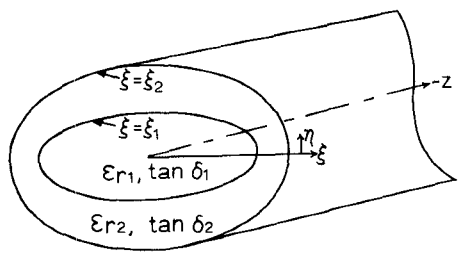

Fig. 1. Dielectric loaded elliptical waveguide and coordinate system.

In this work, the characteristic equations for fast and slow wave modes are solved numerically using accurate computer algorithms to obtain the mode spectrum. Propagation characteristics of the dominant and some higher order modes are studied theoretically, using a computational procedure similar to that employed in [12].

II. Field Components

The geometry of interest is an elliptical metallic waveguide either lined with a dielectric layer or loaded with an elliptical dielectric rod as shown in Fig. 1. The boundary layer between the two dielectric regions is an elliptical surface confocal with the metallic surface. This structure can propagate only hybrid modes which may be either slow or fast waves.

Omitting the t–z dependence, $\exp[j(\omega t-\beta z)]$, where β is the phase coefficient and ω is the angular frequency, the lossless axial field components in region i ($i=1,2$), for even modes are

$$E_{zi}=\sum_{m=1}^{\infty} a_m^{(i)}A_m^{(i)}(\xi,q_i)se_m(\eta,q_i)$$

$$H_{zi}=\sum_{m=0}^{\infty} b_m^{(i)}B_m^{(i)}(\xi,q_i)ce_m(\eta,q_i) \qquad (1)$$

0018-9480/80/1000-1085$00.75